16 April 2012 Volume 100 Number 16

AIP | Applied Physics Letters

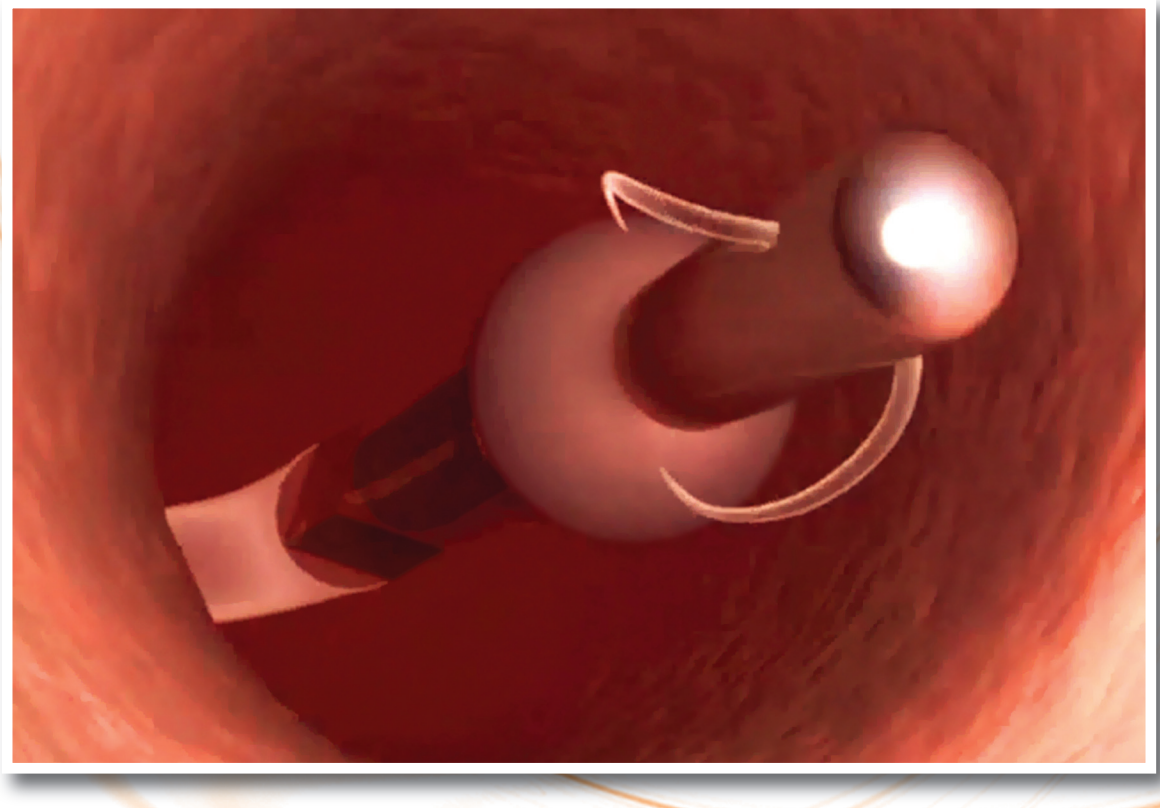

50th Anniversary

apl.aip.org

Multi-degree-of-freedom ultrasonic micromotor for guidewire and catheter navigation: The NeuroGlide actuator

Cheol-Ho Yun,[1] Leslie Y. Yeo,[1] James R. Friend,[1,a)] and Bernard Yan[2]
[1]*Micro/Nanophysics Research Laboratory, The Melbourne Centre for Nanofabrication, Clayton, Victoria 3800, Australia*
[2]*Neurointervention Unit, The Royal Melbourne Hospital, Parkville, Victoria 3052, Australia*

(Received 17 December 2011; accepted 20 January 2012; published online 16 April 2012)

A 240-μm diameter ultrasonic micromotor is presented as a potential solution for an especially difficult task in minimally invasive neurosurgery, navigating a guidewire to an injury in the neurovasculature as the first step of surgery. The peak no-load angular velocity and maximum torque were 600 rad/s and 1.6 nN-m, respectively, and we obtained rotation about all three axes. By using a burst drive scheme, open-loop position and speed control were achieved. The construction method and control scheme proposed in this study remove most of the current limitations in minimally invasive, catheter-based actuation, enabling minimally invasive vascular surgery concepts to be pursued for a broad variety of applications. © *2012 American Institute of Physics*. [http://dx.doi.org/10.1063/1.3702579]

Cerebrovascular disease is the leading cause of long term disability worldwide and a leading cause of death.[1] Minimally invasive vascular surgery (MIVS; Ref. 2) passes a long guidewire through the blood vessel system under x-ray visualization to reach the site of pathology. An endovascular catheter, complete with tools specific to the task, is subsequently guided along the guidewire to the location to treat, for example, strokes, aneurysms, and arterio-venous malformations.[3] The MIVS is often not possible due to the absence of dexterity of the surgeon's tools, the tortuosity of the neurovasculature,[4] and the limited time window within which the surgeon must reach the target location.[5]

To overcome these limitations, we propose an ultrasonic multi-degree of freedom (MDOF) micromotor, the NeuroGlide® actuator for steering the guidewire during navigation. Other approaches have been tried, including magnetic,[6] pull-wire,[7] hydraulic,[8] shape memory alloy,[9] and ionic polymer-metal composite[10] actuators, but they have drawbacks: either requiring a very long time to actuate, which are too large to navigate ~500 μm to 3 mm diameter arteries of the brain distal to the Circle of Willis, and are prone to failure, or offer only poor control.[11] Our aim is to offer a tip that can rotate at least 1 rad/s to offer visible (via x-ray) control to the surgeon and provide 1 nN-m torque about an axis perpendicular to the guidewire to accommodate turning forces as the guidewire is pushed along its route. We arrive at this figure by noting the rotating tip will be about 1 mm long, giving 1 μN of force at the tip upon contact with an artery wall, about what is needed for realistic, 5° deflections of the guidewire tip[12] to properly navigate. Though we aim to have a high-performance motor, a motor that is too powerful is actually dangerous as it can perforate the arterial wall and lead to potentially fatal brain hemorrhage. Piezoelectric ultrasonic microactuators and micromotors[13–15] are attractive for MIVS, offering simplicity, high torque-to-weight ratio, inherent braking, precise positioning accuracy, and flexibility in design.

Most MDOF ultrasonic motors generate rotation about an arbitrary axis by combining the vibrations of a set of orthogonal vibration modes, for example, two orthogonal bending vibration modes and a longitudinal vibration mode,[16–18] each of which are designed to generate rotation about a particular axis. However, in order to generate the three independent vibration modes, at least one ground and four signal input electrodes (and five lead wires each with a diameter of 50 μm) are required; work conducted in our laboratory under our direction by a former student[19] is emblematic of this problem: so many lead wires along the catheter present insurmountable problems in transmission loss, fabrication, and mutual induction losses. Further, controlling the vibration in this system with matched resonance frequencies is impossible due to degeneracy of the bending modes,[20] a phenomenon that has been known for a long time.[21] Worst of all, relying on so many vibration modes in *symmetric* designs is fraught with fabrication problems: Should there be any fabrication mistake or damage during use, the coupling and resonance frequencies can and do change, either causing the motor to stop working or become uncontrollable? At these scales, fabricating such motors for actual applications is simply unrealistic.

Here, we purposely introduce an "error:" a tilt in a component of the structure, making the 240 μm diameter motor far easier to construct and use, because construction flaws become tolerable rather than unsurmountable, and the motor can be operated with only three lead wires. The MDOF motor in Fig. 1 uses only two signal input electrodes attached to two electroded faces of the PZT (C–203 lead zirconate titanate, Fuji Ceramics, Ltd., Tokyo, Japan) along the x axis and a single electrode on the bottom of the PZT element on the z axis; the PZT element itself is polarized along the z-axis direction. Only three wires are necessary for connection. When a sinusoidal voltage potential is applied between one of the x-face electrodes and the ground electrode, both shear and longitudinal strains can be excited simultaneously, deforming the PZT element with transverse bending along the xz plane and axial strain along the z axis due to shear

a)Electronic mail: james.friend@rmit.edu.au.

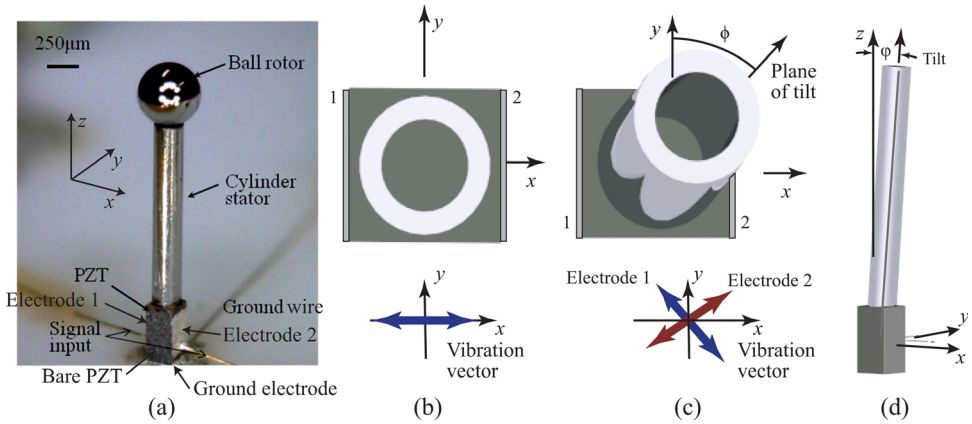

FIG. 1. (a) The motor is reminiscent of our previous simple single-axis motor,[13] but cuts in the tubing are unnecessary here because of the noticeable tilt producing modal coupling. Looking at the stator from the top, without (b) tilt of the tube, the structure is symmetric, and inducing vibration with electrodes 1 and 2 as shown can only generate vibration in the xz plane. If the tube is (c) and (d) tilted by φ in a plane, it is rotated about z by an angle of $\phi \neq 0$ from the positive y-axis, bending vibration about an arbitrary axis may be obtained with only the side electrodes (1,2; also shown in (a)). Taking (d) the page as the plane of tilt, a different view of the amount of tilts, φ, can be shown.

coupling through e_{15} inverse piezoelectric effects.[22] The motion generated by the combined bending and axial deformation of the PZT element causes, likewise, bending and axial deformation in a simple cylinder mounted atop it.

Bending and axial vibration with a temporal phase difference can be simultaneously excited by applying two signals to the side electrodes possessing a temporal phase difference. Because the coupling is via the tilted tube, the input phase difference is not the same as the output phase difference, but the latter may be controlled to obtain elliptical motion at the tip of the stator that, in turn, can be used to rotate an object placed upon the tip. If the tubing of the stator is aligned symmetrically along the z axis (Fig. 1(b)), such elliptical motion of the stator tip can only be generated in the z–x plane, because the stator's bending along the y–z plane is uncoupled from the motion that can be generated with the chosen electrode configuration. However, introducing an asymmetry—the tube's *tilt*—into the structure, it is possible to couple the bending along the y–z plane into the motion generated along the x–z plane, making it possible to drive y–z plane bending vibration through the electrodes on the x-axis faces.[23,24] When the metal cylinder tube is mounted on the PZT with a tilt of ϕ along a direction slightly away from the y-axis and toward the x-axis, as defined by the angle φ, all as shown in Fig. 1(c), the stator's vibrations in the yz-plane are then coupled with vibrations in the xz-plane. Vibration of the stator in the yz-plane can then be generated through excitation of bending vibration in the xz-plane. In this configuration, the vibration vector of the stator tip due to the excitation of "electrode 1" on the positive x-axis face of the PZT element (see Fig. 1(a)) has an orientation along a different plane than when exciting "electrode 2" on the negative x-axis face of the PZT element. By changing the phase between the two electrodes, the orientation of the tip motion can be changed. Using this arrangement, we can control the elliptical vibration direction of the cylinder tip about an arbitrary axis, resulting in arbitrary motion of a rotor placed in contact with this tip.

Modal and harmonic analysis of the stainless steel (304; 240 μm outer and 110 μm inner diameter) stator including a PZT element $250 \times 250 \times 500\,\mu\text{m}^3$ in size, an epoxy bond (7 μm thick) between the PZT and the tube, and Ag/Cr electrodes (15 μm thick) was performed using ANSYS (ANSYS Inc., Canonsburg, PA, USA) to predict the tilted coupling effect. The PZT element size was fixed at $250 \times 250 \times 500\,\mu\text{m}^3$ due to fabrication limitations and the practical need to define the motor's scale for its intended application. The tube was mounted with a tilt of $\varphi = 10^\circ$ in a plane placed at an angle of $\phi = 2^\circ$ from the y-axis and toward the x-axis (see Fig. 1); these angles were selected after exploratory analysis to determine a suitable arrangement that could be reliably fabricated. Though the tilt and the dimensions were constrained due to fabrication limitations, fortunately the simple adjustment of the length was sufficient to permit resonance frequency matching of the first longitudinal, third xz-plane bending, and third yz-plane bending modes at a cylinder length of 1.6 mm as shown in Fig. 2.

Since the cylinder is tilted toward the y-axis and the electrode layer is only present on the x-axis faces of the PZT, the bending stiffnesses of the stator along the xz and yz

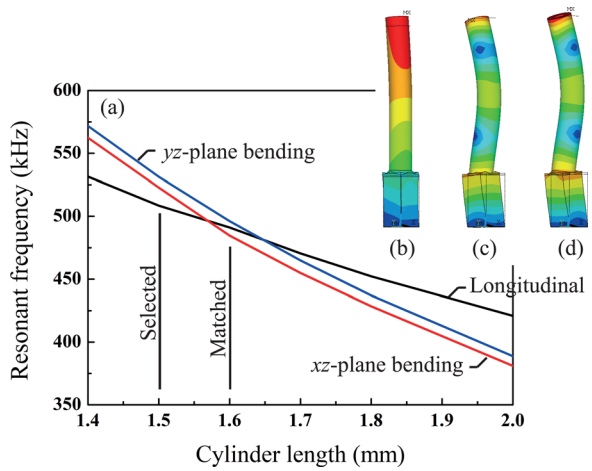

FIG. 2. Changing (a) the cylinder length permits matching of resonance frequencies of the flexural and axial vibrations in the structure at about 1.6 mm. While this is appropriate for a naïve design; choosing this length would result in uncontrollability due to degenerate modes, and so we choose a slightly shorter length of 1.5 mm for the structure to give the (b) first longitudinal, (c) y-axis third bending, and (d) x-axis third bending modes according to analysis.

planes are different. Likewise, the resonance frequencies of the bending modes along these two planes are also expected to be different—the reason for the difference seen in Fig. 2(a), and so precise matching of resonance frequencies is not possible. This is actually desirable, however, and indeed, we chose a cylinder length of 1.5 mm to *increase* the mismatch in resonance frequencies; the mode shapes are illustrated in Figs. 2(c)–2(e). A closely matched resonance system easily causes uncontrollable coupled vibration due to frequency degeneracy as described previously. Each of the modes is not a pure mode of vibration; the longitudinal mode shows some bending as a consequence of the coupling through the tilted stainless steel cylinder. Likewise, each bending mode show longitudinal motion and deflection along planes not parallel to either the x or y axes. Since the tip motions, in particular, are orthogonal and collectively span the entire vector space, rotation of a rotor placed upon the tip about an arbitrary axis is possible with a suitable combination of these vibration modes.

The harmonic response of the stator was calculated from 450 to 550 kHz, spanning the design range for the 1.5 mm tube. The only three resonance peaks to appear were present at 508.5, 522.8, and 531.4 kHz, corresponding to the longitudinal, yz-plane bending, and xz-plane bending vibration mode frequencies, respectively.

The tube was cut by laser machining and mounted on the PZT top using nonconductive epoxy in a painstaking process developed by Watson;[13,25] a completed motor is shown in Fig. 1(a). Drive signals were supplied to the transducer via 50-μm diameter Au wires attached to the PZT electrodes using conductive epoxy (Epotek H20E, Elecsys LLC, USA). A stainless steel ball (ϕ, 0.5 mm), atop the tube in contact along its inner diameter, was retained with a magnetic preload through the presence of a permanent magnet on the bottom of the PZT element. Rotation is generated through stick-slip contact from the elliptical vibration of the stator such that the rotation axis of the ball is generally perpendicular to the plane of the vibration of the stator tip.

The vibration modes and frequency spectrum of the stator tip were measured using a scanning laser Doppler vibrometer (LDV) (Polytec MSA–400, Waldbrunn, Germany) as shown in supplementary material.[30] The yz and xz-plane bending resonances appear in our prototype at 520 kHz and 531 kHz, corresponding to the analytical predictions of 522.8 kHz and 531.4 kHz, respectively. By driving the x-axis electrodes near the yz-plane bending resonance frequency, the yz-plane bending motion can be generated.

Figure 3 shows the measured transient response of the ball rotor velocity along three orthogonal axes with respect to time using a laser Doppler tachometer (Canon LVZ, Tokyo Japan), with a dynamic first-order lag response[26] fitting fairly well, except for an obvious rotor bounce[27] causing oscillation in the response, especially during z-axis rotation. Using Nakamura's method[26] to determine the speed-torque characteristics of the motor for a measured preload of 0.76 mN, the torque is shown over the range of rotation speeds for our system in Fig. 3(b), all at an applied voltage of 15 V_{RMS}.

For many MDOF ultrasonic motors, the direction of rotation is reversed by simply changing the driving phase between the input electrodes. However, not only the direction but also the *axis* of rotation changes when the phase angle between the two electrodes is changed. One has to therefore exercise a bit more care in controlling the motion. At a driving frequency of 518 kHz and a phase difference between the two input electrodes of 20°, the ball rotor rotates along the x-axis. However, the ball rotor spins only in the counter clockwise (CCW) direction. By changing the driving phase, the ball rotor changes its rotation axis direction but rotation in the clockwise (CW) direction along the x-axis was not obtained—the reason for this is not entirely clear, as the vibration behavior indicates CW rotation about the x-axis should be possible. When the phase between the two signal inputs is fixed at 90°, the ball rotor rotates along an arbitrary rotation axis as defined by the driving frequency. However, CCW and CW rotations about the y-axis were obtained at 521 kHz and 531 kHz, respectively. For z-axis rotation, the operating frequencies for CCW and CW directions were 520 kHz and 530 kHz, respectively, all while using a phase difference of 10°. Consequently, rotation about each of the three orthogonal axes x, y, and z can be obtained using specific driving combinations of frequency and phase difference. The maximum torque and rotation speed along the x, y, and z axes were 1.3 nN-m and 400 rad/s, 1.6 nN-m and 600 rad/s, and 0.65 nN-m and 550 rad/s, respectively.

Open-loop control using short-time, high-power sinusoidal *burst drive* signals[20,28] provides a compact method for operating the motor without an impossibly large position

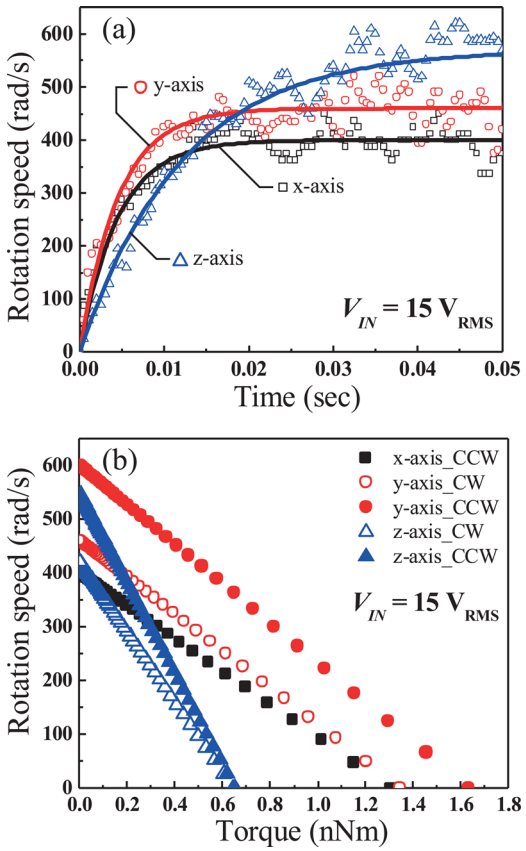

FIG. 3. The (a) transient response of the motor along three orthogonal axes over time, indicating the motor can be operated about all three axes at speeds of at least 350 rad/s with only 15 V_{RMS}. (b) Torque-speed characteristics of the motor at a preload of 0.76 mN and 15 V_{RMS} as determined using Nakamura's method (see Ref. 26).

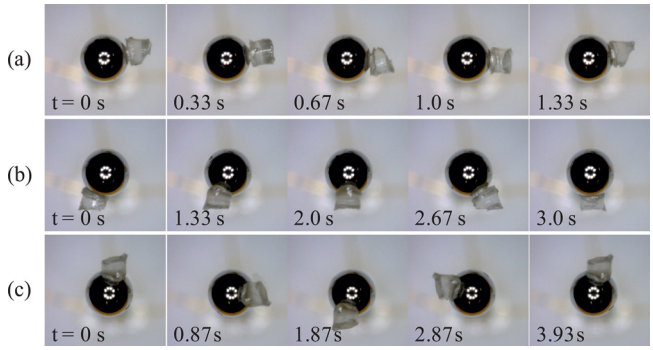

FIG. 4. The operation of the motor at 15 V_{RMS} using an open-loop burst drive scheme: controlled rotation about the (a) *x*-axis, (b) *y*-axis, and (c) *z*-axis. The *x*-axis rotation is shown with 700 wavelengths signal on, followed by 100 000 wavelengths off; the other two rotations are shown with 450 and 100 000 wavelengths on and off, respectively. Each image shows the rotor between input bursts (enhanced online) [URL: http://dx.doi.org/10.1063/1.3702579.1].

sensor placed on the rotor. The rotor displacement is roughly linear with respect to the burst duration of the input signal when the burst duration is shorter than the rise time of the rotor velocity.[29] The operation of the motor using the controlled burst drive scheme is illustrated in Fig. 4.

The ball rotor was operated as a stepping motor about the *x*, *y*, and *z* axes; rotation about an arbitrary axis can be obtained by combining these rotations together in a linear fashion. CCW and CW rotations were possible for the *y* and *z* axes, while CW rotation was possible for the *x* axis; since the rotation speed exceeds 350 rad/s about any axis, the orientation of the rotor can be changed to point at any direction in less than 30 ms even with this limitation, even with the presence of an object on the rotor that prevents its complete rotation as with the small attachment shown on the rotor in Fig. 4. In addition, the rotation speed may be changed by adjusting the burst duration and interpulse interval. In Fig. 4(a), the *x*-axis rotation is much faster than the others, because the burst duration was set to 700 wavelengths. Rotation about an arbitrary axis can be easily obtained by combining discrete combinations of burst signals at the defined frequencies and phases. Expansion of these combinations to other axes and rotation directions is currently under study. Control through the burst drive scheme, though not precise, is likely to be ideal for applications with space limitations sufficient to demand such small motors in the first place, including MIVS.

The authors wish to acknowledge the support of this work by funding provided to them by the NHMRC through Development Grant No. 546238 and the CASS Foundation through Grant No. SM/07/1616.

[1]V. Feigin, C. Lawes, D. Bennett, S. Barker-Collo, and V. Parag, Lancet Neurol. **8**, 355 (2009).
[2]S. Renowden, J. Neurol., Neurosurg. Psychiatry **76**, iii48 (2005).
[3]E. Laws, J. Neuroophthalmol. **28**, 366 (2008).
[4]M. Söderman, D. Babic, R. Homan, and T. Andersson, Neuroradiol. **47**, 735 (2005).
[5]R. Chewning, G. Wyse, and K. Murphy, Semin. Intervent. Radiol. **25**, 42 (2008).
[6]S. Ramcharitar, M. Patterson, R. van Geuns, C. van Meighem, and P. Serruys, Nat. Clin. Pract. Cardiovasc. Med. **5**, 148 (2008).
[7]P. Kanagaratnam, M. Koa-Wing, D. Wallace, A. Goldenberg, N. Peters, and D. Davies, J. Interv. Card. Electrophysiol. **21**, 19 (2008).
[8]K. Ikuta, H. Ichikawa, K. Suzuki, and D. Yajima, in *Proceedings of the 2006 IEEE International Conference on Robotics and Automation, ICRA 2006* (IEEE, 2006), pp. 4161–4166.
[9]K. Park and M. Esashi, J. Microelectromech. Syst. **8**, 349 (2002).
[10]B. Fang, M. Ju, and C. Lin, Sens. Actuators, A **137**, 321 (2007).
[11]Y. Fu, H. Liu, W. Huang, S. Wang, and Z. Liang, Int. J. Med. Robotics Computer Assisted Surg. **5**, 381 (2009).
[12]C. Putman, J. Chaloupka, P. Kailasnath, and J. Alderman, Invest. Radiol. **32**, 241 (1997).
[13]B. Watson, J. Friend, and L. Yeo, J. Micromech. Microeng. **20**, 115018 (2010).
[14]B. Watson, L. Yeo, and J. Friend, Rev. Sci. Instrum. **81**, 063901 (2010).
[15]B. Watson, J. Friend, and L. Yeo, Sens. Actuators, A **152**, 219 (2009).
[16]T. F. Khoo, D. Dang, J. Friend, D. Oetomo, and L. Yeo, IEEE Trans. Ultrason. Ferroelectr. Freq. Control **56**, 1716 (2009).
[17]Y. Gouda, K. Nakamura, and S. Ueha, Ultrasonics **44**, e617 (2006).
[18]H. Kawano, H. Ando, T. Hirahara, C. Yun, and S. Ueha, IEEE Trans. Robotics **21**, 790 (2005).
[19]G. Rogers, J. Micromech. Microeng. **20**, 125002 (2010).
[20]Y. Cheol-Ho, S. Niwano, J. Friend, K. Nakamura, and U. Sadayuki, Jpn. J. Appl. Phys. Part I **42**, 3000 (2003).
[21]S. Hansen and E. Zuazua, SIAM J. Control Optim. **33**, 1357 (1995).
[22]J. Friend and L. Yeo, "Encyclopedia of micro- and nanofluidics," in *Piezoelectric Materials for Microfluidics* (Springer, New York, NY, USA, 2008), pp. 1654–1662.
[23]M. Kurosawa and S. Ueha, J. Acoust. Soc. Am. **90**, 1723 (1991).
[24]M. Aoyagi and Y. Tomikawa, Jpn. J. Appl. Phys. Part I **32**, 4190 (1993).
[25]B. Watson, J. Friend, and L. Yeo, J. Micromech. Microeng. **19**, 022001 (2009).
[26]K. Nakamura, M. Kurosawa, H. Kurebayashi, and S. Ueha, IEEE Trans. Ultrason. Ferroelectr. Freq. Control **38**, 481 (2002).
[27]K.-C. Liu, J. Friend, and L. Yeo, Phys. Rev. E **80**, 046201 (2009).
[28]S. Niwano, C. Yun, J. Friend, K. Nakamura, and T. Ueha, IEICE Technical Report US2003-92 (Institute of Electronics, Information and Communication Engineers, 2003), Vol. 103, p. 43.
[29]W. Kim, C. Yun, and S. Lee, Jpn. J. Appl. Phys. **47**, 5687 (2008).
[30]See supplementary material at http://dx.doi.org/10.1063/1.3702579 for information on laser Doppler vibrometry used to determine the vibration shapes of the stator in this motor prototype as it undergoes different driving configurations.